

Quantum Two-Body Interactions in Harmonic Traps and a Study of Dynamic Optical Lattices

Michael Roberts

American University Honors Capstone

Advisors: Profs. P. R. Johnson and N. L. Harhsman

Additional Collaboration: Prof. J. Uscinski

December 19, 2011

Abstract

This paper is divided into two parts. The first is an investigation of the effects of tunable interactions between two ultracold neutral bosons confined by a quantum harmonic oscillator trap. As the demand for experimental study of quantum systems grows stronger, it is of keen interest to predict and control their behavior. Specifically, we explore the relation between the strength of interactions and speed of the interaction ramping time scale on the excitation of two-body states, and explain how such states are surprisingly resistant to perturbations. The second part of this paper describes a fully controllable dynamic optical lattice. These lattices are the skeleton that hold ultracold particles in manipulable arrays so that quantum, solid state, and condensed matter phenomena can be observed in a controlled environment.

1 Part I: Two-Particle Interaction in a Harmonic Trap

1.1 Analytic Framework

A system of two identical non-interacting particles in a one-dimensional quantum harmonic trap (QHO) potential

$$V(x_1, x_2) = \frac{1}{2}m\omega^2(x_1^2 + x_2^2) \tag{1}$$

can be characterized by the position-space Hamiltonian

$$\hat{H}_{QHO} = \hat{K} + \hat{V} = \frac{-\hbar}{2m} \left(\frac{\partial^2}{\partial x_1^2} + \frac{\partial^2}{\partial x_2^2} \right) + \frac{1}{2} m \omega^2 (x_1^2 + x_2^2). \quad (2)$$

Although the true interaction potential may be complicated, for ultracold interactions we can approximate the potential by a zero-range Dirac delta function $V_{int} = G(t)\delta(x_2 - x_1)$ [1, 2] which is scaled by a time-dependent interaction strength parameter $G(t)$, where $G > 0$ represents particle repulsion and $G < 0$ represents mutual attraction. The interaction strength between otherwise neutral particles can be finely tuned by manipulation of external magnetic fields [3], known as Feshbach resonances. The mechanisms responsible for this phenomena will not be discussed in this paper, and the interaction strength G will be treated as arbitrarily controlled.

Including the zero-range interaction, the perturbed time-dependent Hamiltonian describing the system is

$$\hat{H} = \frac{-\hbar}{2m} \left(\frac{\partial^2}{\partial x_1^2} + \frac{\partial^2}{\partial x_2^2} \right) + \frac{1}{2} m \omega^2 (x_1^2 + x_2^2) + G(t)\delta(x_1 - x_2) \quad (3)$$

from which the evolution of the quantum state is determined by solving the Schrödinger equation

$$i\hbar \frac{\partial}{\partial t} \Psi = \hat{H} \Psi. \quad (4)$$

The steady-state solutions to Eqn. 4 for $G(t) = 0$ are the well known solutions to \hat{H}_{QHO} ,

$$\psi_{QHO n_1 n_2} = \sqrt{\frac{m\omega}{\pi \hbar 2^{n_1+n_2} n_1! n_2!}} e^{-m\omega(x_1^2+x_2^2)/2\hbar} H_{n_1} \left(\sqrt{\frac{m\omega}{\hbar}} x_1 \right) H_{n_2} \left(\sqrt{\frac{m\omega}{\hbar}} x_2 \right), \quad (5)$$

with quantized energies

$$E_{n_1 n_2} = E_{n_1} + E_{n_2} = \hbar\omega(1 + n_1 + n_2) \quad (6)$$

where $n_1, n_2 \in \mathbb{Z}^{++}$ and H_n are the Hermite polynomials.

Returning to Eqn. 3, we change bases to center of mass X and relative x coordinates. Let

$$X = \alpha(x_1 + x_2) \text{ and } x = \alpha(x_1 - x_2) \quad (7)$$

be the new coordinates of the center of mass (COM) and relative positions, respectively, which are scaled in natural units of α where

$$\alpha = \sqrt{\frac{m\omega}{2\hbar}} \quad (8)$$

Applying this change to the basis set ($\{x_1, x_2\} \rightarrow \{X, x\}$), we derive a new dimensionless Hamiltonian in units of $\hbar\omega$:

$$\frac{\widehat{H}}{\hbar\omega} \equiv \widehat{\widetilde{H}} = -\frac{1}{2}\left(\frac{\partial^2}{\partial X^2} + \frac{\partial^2}{\partial x^2}\right) + \frac{1}{2}(X^2 + x^2) + \gamma(t)\delta(x). \quad (9)$$

Here, we have reparameterized the interaction strength as $\gamma(t) = \frac{\alpha G(t)}{\hbar\omega}$. $\widehat{\widetilde{H}}$ is a superposition of two Hamiltonians: the non-interaction harmonic oscillator in COM X space and a harmonic oscillator perturbed by the interaction $\gamma\delta(x)$ in relative x space. The Hamiltonian solutions can be broken down via the separation of variables ansatz $\psi(x, X) = u(x)\Upsilon(X)$. If we treat the interaction parameter as fixed, we can solve the time-independent Schrodinger equation $\widehat{\widetilde{H}}\psi = E\psi$.

The COM steady state solutions Υ_n are the same as those in Eq. 5, but are now reduced to naturalized units in one variable:

$$\Upsilon_n(X) = (2^n n! \sqrt{\pi})^{-1/2} e^{-X^2/2} H_n(X), \quad (10)$$

with dimensionless energies $E_n = n + 1/2$. Because the COM wavefunction is not dependent on the interaction parameter γ , it will remain in its initial state. In this way, the COM can be ignored when evaluating the effects of particle interactions, but can always be multiplied by the relative space wavefunction to recover the full 2D wavefunction.

Returning to the relative space Hamiltonian, we first note that for any value of γ , the overall potential only changes at the origin $x = 0$. At this location, all odd harmonic states vanish, and therefore will not be affected by the presence of the interaction potential, so long as it exists only at the origin. Therefore, the relative space Hamiltonian has the same odd-symmetry states as the harmonic trap (in naturalized units):

$$u_{n,odd}(x) = (2^n n! \sqrt{\pi})^{-1/2} e^{-x^2/2} H_n(x) \quad (11)$$

with dimensionless energies $\varepsilon_{n,odd} = n + 1/2$.

The even state solutions are [4]:

$$u_{n,even}(x) = N_n U\left(\frac{1 - 2\varepsilon_n}{4}, \frac{1}{2}, x^2\right) e^{-x^2/2}, \quad (12)$$

where the Tricomi Functions $U(a, b, z)$ take over the roll of the Hermite polynomials¹, and N_n is the dynamic normalization factor² [5]. The even eigen-energies must be found numerically through the implicit relation³:

¹In fact, the Hermite polynomials are a subset of Tricomi functions for specific values of ε : the QHO steady state eigenvalue energies.

²See Appendix A, *Normalization Factor*.

³The function Γ is the factorial function extended to the entire real line.

$$\frac{\gamma}{\Gamma(\frac{3-2\varepsilon_n}{4})} = \frac{-2}{\Gamma(\frac{1-2\varepsilon_n}{4})} \quad (13)$$

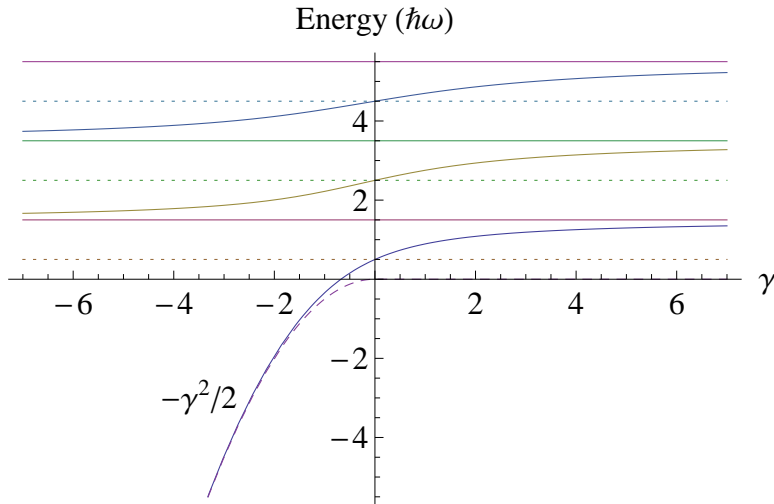


Figure 1: Plot of the energy as a function of interaction strength γ for the $n = 0$ to $n = 5$ states.

The graph of the energy of each stationary state versus the interaction parameter (Figure 1) is immensely interesting in and of itself. At $\gamma = 0$, we have the expected energies at integer increments starting at the ground state energy of $\frac{1}{2}$. However, as γ increases (representing stronger and stronger repulsion), the energy of each even state tends toward the energy of the odd state directly above it. The exact opposite is true for attractive interactions: as γ goes to increasingly negative values, the even energies asymptote towards the odd states directly below. However, the symmetry of this graph is broken by the behavior of the ground state, which as the name implies, has no state beneath it. As $\gamma \rightarrow -\infty$, the ground state energy falls unbounded in the mathematical sense, representing an infinitely bounded state in the physical sense. The deeper implications behind this phenomenon are not entirely understood. However, the rapidity of the divergence suggests that the ground state of the relative wavefunction quickly condenses into a strong cusp, becoming sharper and sharper at the origin. Recalling the classic example of a bound particle in an infinite Dirac well, but subject to no other potential, we see that the ground state, as gamma grows increasingly negative, quickly "forgets" the presence of the harmonic trap and approaches this textbook case. Figure 1 agrees with this evaluation, showing that the ground state energy rapidly approaches $-\gamma^2/2$, the ground state energy of a wavefunction experiencing only an infinite narrow well.

In addition to the shared energy values, the extreme interaction strengths also force the

even wavefunctions into the same configuration as the corresponding odd state⁴. Technically, the even state wavefunctions are identical to the absolute value of the odd state wavefunctions, but the physically observable probability densities (the square of the absolute value of the wavefunction) are the same.

$$\lim_{\gamma \rightarrow \pm\infty} |\psi_n|^2 = |\psi_{n\pm 1}|^2, n \in \{2, 4, 6\dots\} \quad (14)$$

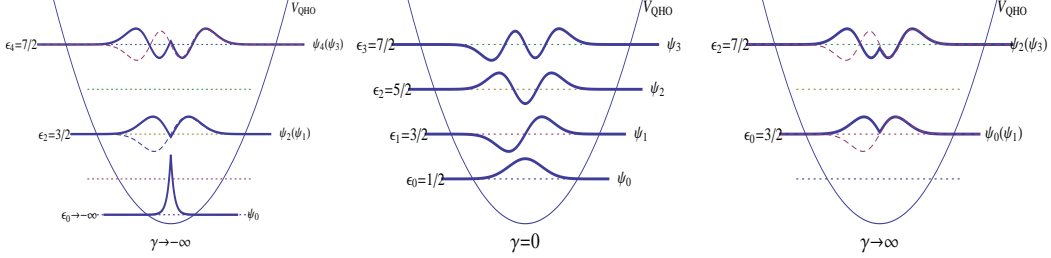


Figure 2: Plots of the first few steady states for $\gamma = -\infty$, $\gamma = 0$ and $\gamma = \infty$.

1.2 Numeric Framework

We have explored the concepts put forth in this paper by a numeric technique known as the split-operator method (SOM). In order to solve Schrödinger's equation for the evolution of a quantum state in a dynamic potential, the complications of solving a partial differential equation in time and space renders nearly all possible scenarios unexplorable. The goal of this method is to reanalyze the time-dependent Schrödinger equation for small time steps t_j separated by Δt to create a discrete evolution:

$$\widehat{U}\Psi(x, t_{j+1} = t_j + \Delta t) = e^{-i\widehat{H}\Delta t/\hbar}\Psi(x, t_j). \quad (15)$$

We begin with the standard quantum unitary evolution operator

$$\widehat{U} = e^{-i\widehat{H}\Delta t/\hbar} = e^{-i(\widehat{K}+\widehat{V})\Delta t/\hbar}, \quad (16)$$

which is a rotation in Hilbert Space \mathcal{H} for the state $|\Psi\rangle \in \mathcal{H}$ on which it acts: $\widehat{U}|\Psi\rangle = |\Psi'\rangle$. The Baker-Hausdorff-Campbell theorem allows us to factor \widehat{U} as

$$\widehat{U} = e^{-i(\widehat{K}+\widehat{V})\Delta t/\hbar} = e^{-i\widehat{K}\Delta t/\hbar}e^{-i\widehat{V}\Delta t/\hbar} + \mathcal{O}(\Delta t^2). \quad (17)$$

The $\mathcal{O}(\Delta t^2)$ correction is due to the non-commutativity of \widehat{V} and \widehat{K} . We can take this factorization one step further and write a "split" evolutionary operator [6]:

⁴This includes the ground state being forced into the first excited state as $\gamma \rightarrow \infty$.

$$\widehat{U} = e^{-i\widehat{K}\Delta t/2\hbar} e^{-i\widehat{V}\Delta t/\hbar} e^{-i\widehat{K}\Delta t/2\hbar} + \mathcal{O}(\Delta t^3). \quad (18)$$

Let us define $\widehat{U}\widehat{K}_{1/2} \equiv e^{-i\widehat{K}\Delta t/2\hbar}$ and $\widehat{U}\widehat{V} \equiv e^{-i\widehat{V}\Delta t/\hbar}$ for a compact notation.

We note that the discretization of t results in an error accumulation on the order of $\mathcal{O}(\Delta t^3)$ per time step[7]. After $N_t = \frac{T}{\Delta t}$ timesteps, where T is the total evolution time, the error accumulated is $\mathcal{O}(\Delta t^2)$.

We begin by defining a position space grid $\{x_n = x_{\min} + (n-1)\Delta x\}$ where $n \in 1, 2, \dots, N_g$ and N_g is the number of gridpoints sampled, i.e. the grid resolution [8]. We can imagine this as a periodic space with circumference L_x such that $x_{\max} + \Delta x = x_{\min}$ and $\Delta x = L_x/N_g$. We also define a momentum space grid $\{p_m = 2\pi m/L_x\}$, $m \in 1, 2, \dots, N_g$. The momentum space must match the conditions presented by the position space; specifically: $p_{\max} + \Delta p = p_{\min}$, $\Delta p = 2\pi/L_x$, and $L_p = \Delta p N_g$.

The relationship between position and momentum space is found via the Fourier Transform⁵. Let $\psi(x)$ be a position-space wavefunction, and $\tilde{\psi}(p)$ be the corresponding momentum-space wavefunction. Then:

$$\tilde{\psi} = \mathcal{F}\psi = \frac{1}{\sqrt{2\pi}} \int_{-\infty}^{\infty} \psi e^{-ipx} dx. \quad (19)$$

The overall quantum state Ψ can be represented as a vector in a N_g -dimensional Hilbert space $|\Psi\rangle \in \mathcal{H}_{N_g}$ which can be represented in position-space by taking the projection of Ψ on the position-space bases

$$\psi(x_i) = \langle x_i | \Psi \rangle, \quad (20)$$

or conversely in momentum-space

$$\tilde{\psi}(p_i) = \langle p_i | \Psi \rangle. \quad (21)$$

Because our method of evolution operates on discretized variables, we must use a discrete version of the Fourier Transform (DFT). However, because in the discrete case the transform operator is defined as a matrix with dimension $N_g \times N_g$, the number of sub-operations executed scales as N_g^2 each time the DFT is invoked. For this reason, an alternative was developed known as the Fast Fourier Transform (FFT) which is a highly accurate approximation to the DFT, but scales as $N_g \log N_g$, making it much faster.

The motivation behind being able to transform between position and momentum-space is not immediately obvious, especially when this transformation creates additional operations to be executed during the evaluation period. Recalling Eq. 18, each time step of the

⁵To a true mathematician, Eq. 19 is actually the *inverse* Fourier transform.

evolution approximation involves acting on the previous wavefunction with three unitary energy operators: a kinetic energy operator, a potential energy operator, and another kinetic energy operator. The potential energy operator is defined by

$$\widehat{V} = V(\widehat{x}) = V(x), \quad (22)$$

which is the potential energy of the system in position-space (where $\widehat{x} = x$). The kinetic energy operator is defined:

$$\widehat{K} = \frac{\widehat{p}^2}{2m} = \frac{-\hbar^2}{2m} \frac{\partial^2}{\partial x^2} \quad (23)$$

in position-space, which is derived from the relation $\widehat{p} = -i\hbar \frac{\partial}{\partial x}$. However, in momentum-space, $\widehat{p} = p$, and the kinetic energy operator is defined:

$$\widehat{K} = \frac{p^2}{2m} \quad (24)$$

In position-space, the kinetic energy operator is proportional to the Laplacian ∇^2 on position base states. The derivative operator can be approximated by a $N_G \times N_G$ matrix, but this approach scales as N_G^2 for each application of \widehat{K} . However, in momentum-space, the kinetic energy operator is simply a multiplicative operation, and therefore scales only as N_G . For this reason, it uses fewer resources to implement this operator in momentum-space, after a FFT.

Combining these, we can create a chain of operators that evolve the wavefunction $\Psi(x, t) \rightarrow \Psi(x, t + \Delta t)$:

$$\Psi(x, t + \Delta t) = \mathcal{F}^{-1} * \widehat{U}K_{1/2} * \mathcal{F} * \widehat{U}V * \mathcal{F}^{-1} * \widehat{U}K_{1/2} * \mathcal{F} * \Psi(x, t). \quad (25)$$

Although aesthetically this form is convoluted, computationally it creates an efficient and powerful approximating method which scales as $N_G \log N_G$ and has error $\mathcal{O}(\Delta t^3)$.

In the discrete representation, there are also complications that arise from the use of the Dirac spike, which is infinitesimal in width. Although this powerful tool is often used in mathematical frameworks on account of its convenient properties, it is more realistic to use an interaction potential that extends with finite width. We therefore chose to use a narrow Gaussian function to represent a finite-range interaction potential

$$Int(x) = \gamma e^{-x^2/2\lambda^2}, \quad (26)$$

where $\lambda \ll \sigma$. The length scale of the interaction potential λ is much smaller than the length scale of the trap σ .

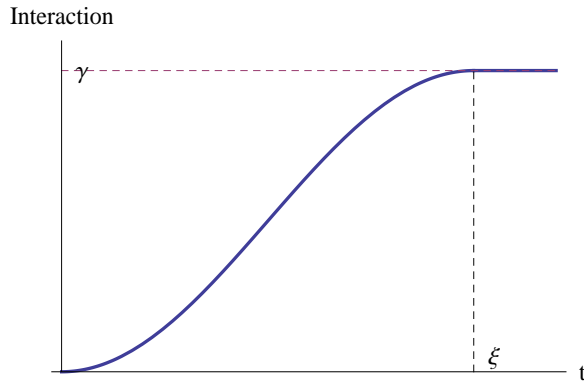


Figure 3: Plot of the interaction ramping with time, where ξ is the ramp period.

The ramping of the interaction strength can also lead to non-stationary behavior in the numeric state. Ramping "kinks" (discontinuities in the first derivative) can create perturbations in the wavefunction, but the use of smoothed ramping functions requires additional criteria for deciding when the interaction strength is "sufficiently close" to the limiting value. We decided to use a shifted sine function during the ramp period ξ . In this way, we avoid both kinks and limiting behaviors, at the expense of a discontinuity in the third derivative. The ramping function has the form

$$Int(x, t) = \begin{cases} 0 & t < 0 \\ \gamma e^{-x^2/2\lambda^2} \frac{1}{2} [\sin(\frac{\pi t}{\xi} - \frac{\pi}{2}) + 1] & 0 \leq t \leq \xi \\ \gamma & \xi < t \end{cases} . \quad (27)$$

1.3 Numeric Validity

The obvious problem in dealing with numeric analyses is the interpretation of the accuracy of the results. How can we be sure what the computer generates is physically meaningful? One solution is to apply a test case in which the result is known analytically, and then adjust the computational parameters until the numeric result matches the analytic solutions. Although the trivial case is to apply this approach to an unchanging QHO potential, the triviality of this case does not strongly test the numerical implementation.

A better test is to observe the case of a highly adiabatic dynamic potential to a steady state solution for some arbitrary nonzero choice of γ . We expect that if we ramp up the interaction strength infinitely slowly, we will remain in the ground state the entire time, even though the form of the ground state changes with γ ⁶. For our test case, we evolved the

⁶For example, if we began in the $|\psi_0\rangle$ ground state when $\gamma = 0$ and ramped infinitely slowly to $\gamma = \gamma_o \neq 0$, we would expect to remain perfectly in the state $|\psi_0\rangle$ even though $|\psi_0\rangle_{\gamma=0} \neq |\psi_0\rangle_{\gamma=\gamma_o}$. This is the perfectly

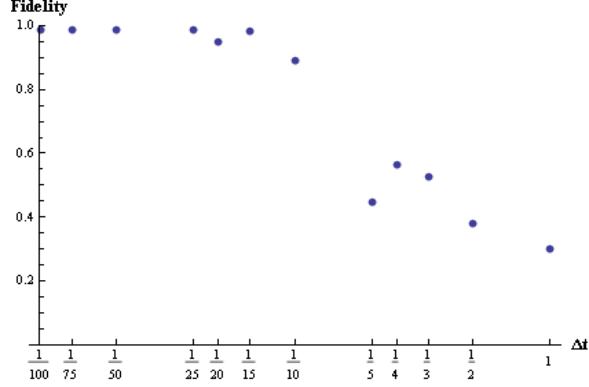


Figure 4: Plot of the fidelity of the analytic ground state $|0\rangle$ and numeric state $|N\rangle$ for various Δt at $N_g = 500(\Delta x = \frac{1}{50})$ and $\xi = 10, \gamma = 10$. Saturation is reached at $\Delta t = \frac{1}{75}$, at which point $\langle N|0\rangle = .9893$.

ground state at $\gamma = 10$ over a ramping period of $\xi = 10 \gg \frac{1}{\omega}$, where $\frac{1}{\omega}$ is the characteristic time scale of the quantum trap, to approximate an adiabatic ramp time. We compared the fidelity of the resulting numeric wavefunction $|N\rangle$ to the analytic ground state $|0\rangle$ of the $\gamma = 10$ interaction potential, where

$$F(\alpha, \beta) = |\langle \alpha | \beta \rangle|, \quad (28)$$

(the overlap between the two states,) and then increased the number of time and spacial sampling points (resolution) until the fidelity value becomes insensitive to increasing resolution. This assures us that any significant difference in the fidelity is attributable to physical effects, not computational errors.

1.4 Results

Collectively, the results of our tests indicate that even when subject to varying potentials, the evolving numeric wavefunction $|N\rangle$ is resistant to excitations. That is, if $|N\rangle$ began in the ground state, it retains a strong tendency to remain in the ground state throughout the ramping process. This tendency is weakened by decreasing dramatically the ramp period ξ or increasing the magnitude of the interaction strength $|\gamma|$. The sensitivity to positive versus negative γ is not the same; the resistance to excitations is weaker for $\gamma < 0$ than for $\gamma > 0$.

First we examine the effect created by varying the interaction strength. Referring to Figure 5, we see that as the ramping period becomes longer, the probability of finding $|N\rangle$

adiabatic scenario.

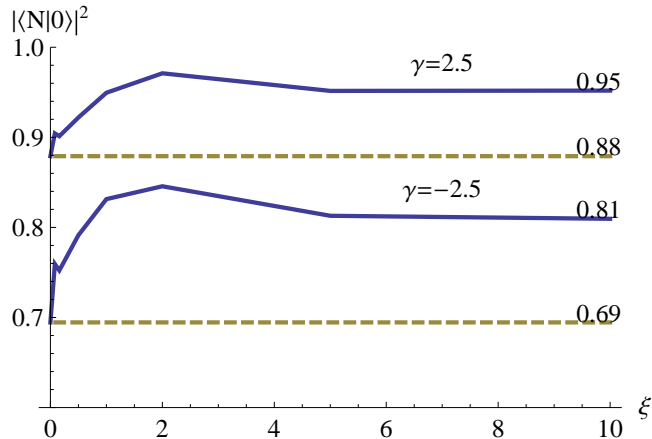


Figure 5: The probability of finding $|N\rangle$ in the ground state as a function of ramp period ξ for $\gamma = \pm 2.5$. Though they mirror one another in behavior, the attractive interaction displays greater probability of excitation. The dashed lines show the minimal possible probability for each scenario, occurring at instantaneous interaction ramping $\xi = 0$.

in the ground state ($P = |\langle N | 0 \rangle|^2$, where $|0\rangle$ is the analytic ground state) is increased, mimicking the increasingly adiabatic case. From the figure, it is apparent that this probability does not approach one, which indicates statistical error. We estimate that there are two possible sources. The first is the general disagreement created through the numerical approximations. We estimate this systematic error to be about 3%. Observed "overshoots" of the total probability of eigenstates never exceeded 1.03, 3% above the physically acceptable value of one, when taking into account the first six states. The second factor of error is the model itself. The difference between a delta spike and a narrow Gaussian, though small, can lead to differing behaviors among the occupying wavefunctions. This is not a source of error in the true sense; we are merely comparing the results of one physical model to a similar second model.

Figure 5 also shows how the behaviors of specific γ are not symmetric with respect to the sign of γ . The plot shows that the behavior of $\gamma = -2.5$ follows closely in form of $\gamma = 2.5$, but that the physical probabilities are decreased for negative γ . This indicates that there is a significant underlying difference in the behavior of the ground state for attractive interactions and repulsive interactions.

We also observe snapshots of the numeric state for varying interaction strengths at specific values of the ramp period. Figure 6 shows how, as expected, the probability of finding $|N\rangle$ in the ground state drops off as the magnitude of γ increases. Again, the disparity between repulsive and attractive interactions is observed, as this probability drops off much faster for negative γ . Also, as we expected, the slower the interaction is turned

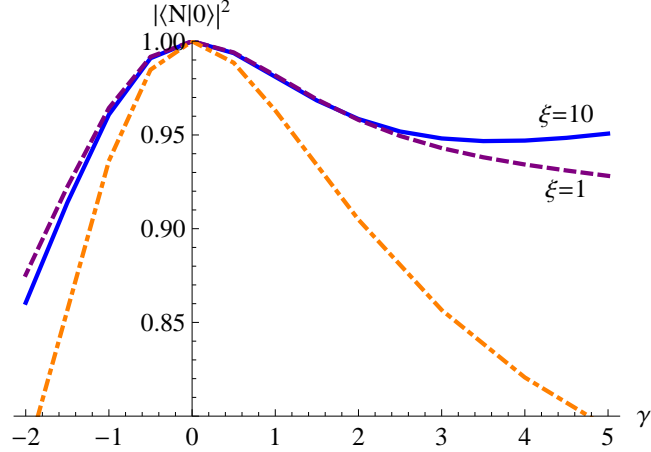


Figure 6: The probability of finding $|N\rangle$ in the ground state as a function of interaction strength γ for ramp periods of $\xi = 1$ (solid,) and 10 (dashed.) The probabilities drop off much faster for attractive interactions than repulsive. The dot-dashed line shows the instantaneous ramping case, the minimum allowable probability for any ξ, γ .

on, the slower this probability drops off, but only for positive γ . For negative γ , the faster ramping has the lower probability fall off. The difference between the two is small, and may be an artifact of numeric error. Additional comparisons of a greater set of ramp speeds is needed to draw any further conclusions.

The dot-dashed line shows the instantaneous ramping case, $\xi = 0$. This probability is found by comparing the analytic ground state for any γ with the QHO ground state $\gamma = 0$. The latter represents instantaneous ramping, such that the wavefunction has no time to evolve. Even up to interaction strengths of $\gamma = 5$, the minimal probability of finding the wavefunction in the ground state is .79. This obviously is not true for negative γ where the probability drops of faster, but this is definitive evidence that the state is resistant to excitations even for fast interaction ramping and up to large interaction strengths.

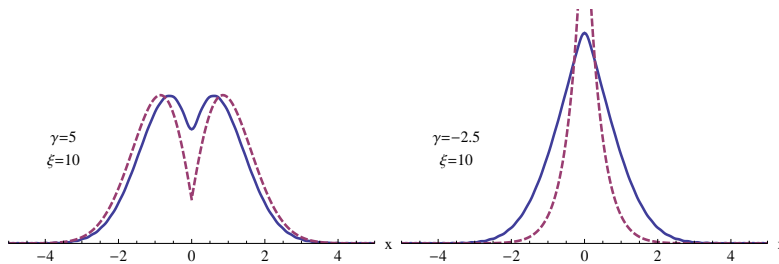


Figure 7: Plots of the evolved numeric wavefunctions $|N\rangle$ (solid) transposed on the analytic ground state wavefunctions $|0\rangle$ (dashed) for various interaction strengths.

1.5 Additional Research

The field of quantum information theory is a hot area right now. A key topic of interest to researchers in this field is the understanding and exploitation of quantum entanglement. Entanglement, in its most rudimentary form, is a measure of correlation of information between two observable systems. For this paper, the entanglement might be between the positions of particle 1 and particle 2. Conversely, it might be the correlation between the center of mass and relative positions. In fact, each particular coordinate system chosen can exhibit entanglement measures and, interestingly enough, not every coordinate system will have the same measure.

There are many people who study how the various entanglements among coordinate transformations reflect symmetry properties in the physical systems in those coordinates. For example, using the purity (one type of entanglement measure)

$$P(\phi) = \int \int \int \int_{\mathbb{R}} \phi(x_1, x_2) \phi^*(x'_1, x_2) \phi^*(x_1, x'_2) \phi(x'_1, x'_2) dx_1 dx_2 dx'_1 dx'_2, \quad (29)$$

we can determine how the interaction between the particles entangles their positions (or momenta, etc.) It is easily shown that any separable wavefunction $\phi(x, X) = \phi_x(x) \phi_X(X)$, such as that of the COM-relative basis wavefunction used in this paper, has a purity of one and is perfectly unentangled for any value of γ . However, in the original position-space basis, this is not true. (Numerically, it is roughly 0.7 for $\gamma = 5$.)

Future research studying how the interaction affects entanglement could show how entanglement can be directly tuned. We conjecture that as γ becomes more negative, and the particles more attracted, the entanglement between the particles' positions should become increasingly correlated.

2 Part II: The Idealized Three-Dimensional Optical Lattice

More often than not, physicists in the laboratory are operating under monetary as well as equipment limitations. Because of this, lab technicians construct their particular lattice to fulfill only the specific needs of their experiment which has lead to a shortage of information of the full abilities of the optical lattice. However, through the use of computer simulation, we can study the various configurations that a perfectly controllable lattice can perform.⁷

2.1 Defining the Potential

A fully controllable lattice consists of three independent lasers, all aimed orthogonally at a single intersection point and retroreflected back upon themselves. Each beam is an electromagnetic wave travelling in the \hat{e}_1 -direction with polarizations in the \hat{e}_2 - and \hat{e}_3 -directions. For example,

$$\vec{E}_1 = \sum_{\{i=2,3\}} [E_{1i} e^{i(ky - \omega t + \phi_{1i})} \hat{e}_i + E_{1i} e^{i(-ky - \omega t + \theta_{1i} + \phi_{1i})} \hat{e}_i], \quad (30)$$

where the subscripts mn signify the the beam direction, m , and the polarization direction, n ; ϕ represents the incident phase of the beam and θ represents an arbitrary phase change of the beam post reflection; k represents the wave number; and ω represents the angular frequency of the wave. The intensity of each orthogonal component of each beam can be independently controlled. By controlling these components' strengths we can effectively induce a polarization rotation. The net electric field of the lattice is the sum of these three beams:

$$\vec{E} = \sum_{i=1}^3 \vec{E}_i \quad (31)$$

Particles in such a field experience an effect known as a scalar light shift depending on the average intensity of the field:

$$I_{avg} \propto \left| \vec{E}_{tot} \right|^2 = \vec{E}_{tot} \cdot \vec{E}_{tot}^* \quad (32)$$

The average intensity of the field is only stable (naturally time-independent) if the wavelengths and wavenumbers of the three beams are identical. Otherwise, vibrational oscillations arise in the intensity, which will destabilize the lattice. This leaves the incident phase, relative phase, and individual beam intensity as controllable parameters.

⁷For additional information, see [9], [10], and [11].

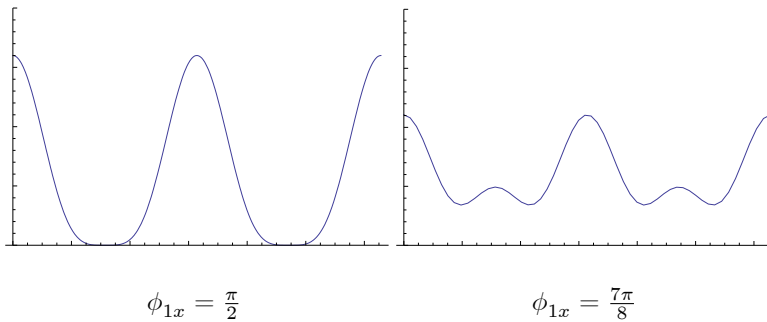
The physical lattice is created by the average intensity field derived in Eq. 32. Using a frequency just below the resonant frequency of the lattice particles, we create red-detuning. In a red-detuned lattice, the locations of maximum intensity correspond to potential minima; particles are drawn toward high-intensity sites. (The opposite effect is known as blue-detuning.)

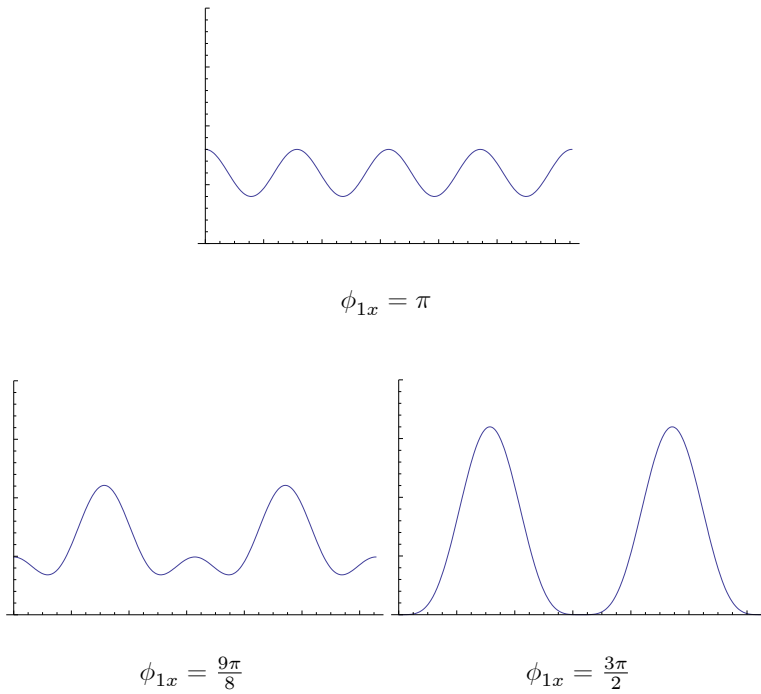
2.2 Basic Parameters

In total, the lattice has 18 controllable parameters: six intensities (where $I_{ij} = E_{ij}^2$) which control the amplitudes of the beams (and effectively the polarization angles), six initial phases ϕ_{ij} , and six phases θ_{ij} (for example, the beam projected in the y-direction has a phase change for both its x- and z-polarized components.) By examining the final intensity, it can be seen that the ϕ parameters only exist in pairs. By exploiting this, we can eliminate half of the ϕ values. As an arbitrary choice, we let the ϕ parameters of higher numeric index be eliminated.

2.3 1D Well Splitting and Pairing

Consider the 1D (blue-detuned) lattice where the periodic wells are slowly split into two equal wells, pair with neighboring wells, split again, then rejoin to create the original well again. This lattice set can be constructed along the y-axis (at $x = z = \frac{\pi}{2}$) by letting $I_{1x} = I_{3x} \neq 0$, $\theta_{3x} = \pi$, $\phi_{1x} = \frac{\pi}{2}$, and letting ϕ_{1x} increase slowly enough to maintain stability in the lattice. The following graphs plot intensity as a function of position.





The ability to divide wells is of key importance to technologies using atom interferometry. By splitting the atomic wavefunction into separate wells, the differences between the two wavefunctions can be analyzed to measure minute effects of the surrounding environment, such as tiny variations in gravity. This could ultimately lead to abilities such as advanced GPS.

2.4 Basic 2D Configurations [9]

We can first ignore the effects of the third beam, such that we are effectively dealing with a 2D lattice in the xy -plane. The first 2D lattice we consider is when beams 1 and 2 are polarized in the same direction, in this case \hat{z} (see Figure 2.1-A). This creates a lattice of wells that are aligned along a diagonal (the intensity is roughly sinusoidal in the direction $(\hat{x} + \hat{y})/\sqrt{2}$.)

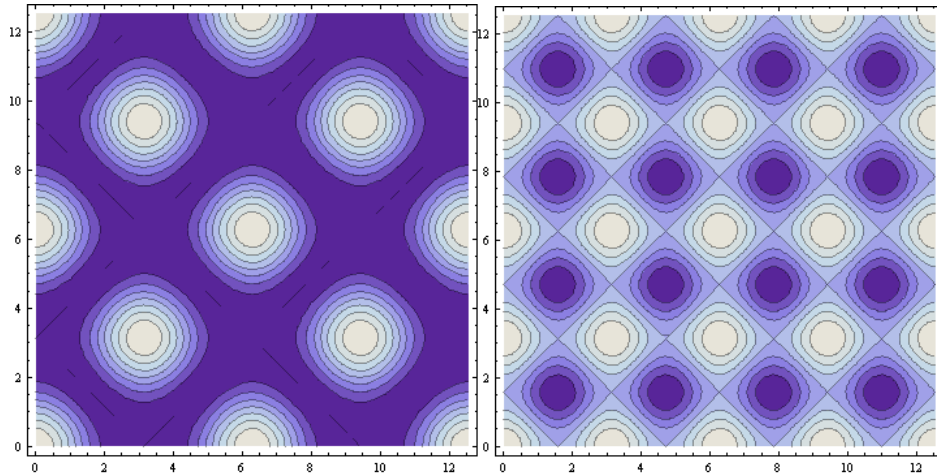


Figure 2.1-A

Figure 2.1-B

The second 2D lattice we examine is the case in which the beam polarizations are orthogonal: beam 1 only has \hat{x} polarization and beam 2 only has \hat{y} (Figure 2.1-B). This lattice has wells that are arranged rectangularly. As shown, it has more, but shallower, wells than the previous lattice. In both graphs, lighter colors corresponds to higher intensity. For the purposes of well pairing in 2D, it is a combination of these two lattice types that allows for this ability.

2.5 Basic 3D Configurations

The simplest 3D lattice structure we consider is the case in which all three beams are polarized orthogonally; that is, beam 1 is polarized in the \hat{z} -direction, beam 2 in the \hat{y} , and beam 3 in the \hat{x} -direction. This setup gives a sinusoidally varying intensity in all three directions. If all phase parameters vanish, and $I_{1z} = I_{2y} = I_{3x} \neq 0$, then the lattice is a simple-cubic crystal of equally-deep wells (Figure 2.2-A).

The next simple case we consider is when all beams have equal intensities. (That is, $I_{1x} = I_{1z} = I_{2x} = I_{2z} = I_{3x} = I_{3y} \neq 0$.) This creates a body-centered cubic lattice with wells roughly twice as deep as the previous setup (Figure 2.2-B). (Contours shown in each frame are not equal in value.)

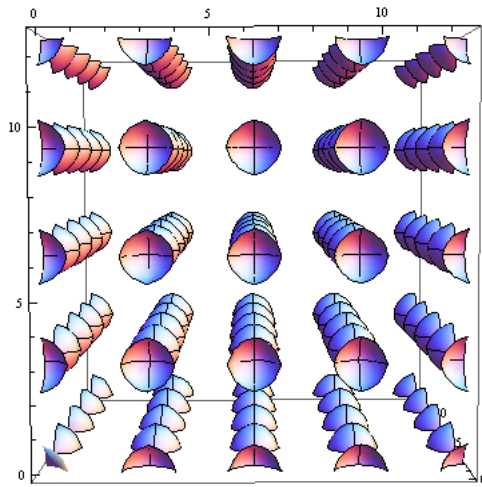


Figure 2.2-A

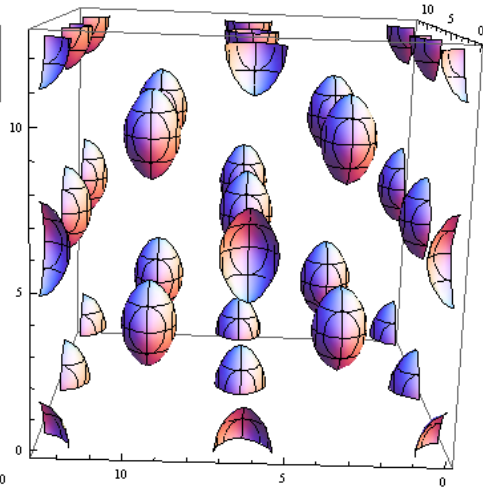
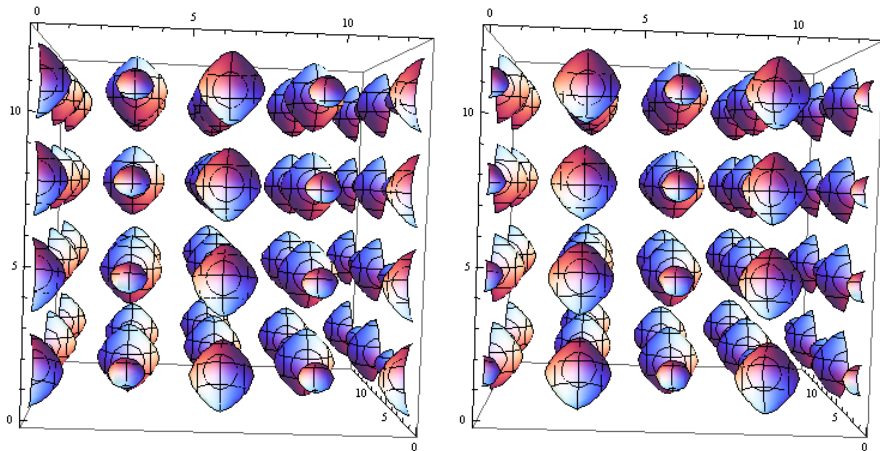


Figure 2.2-B

However, as stated before, the ideal configuration for well-pairing transformations is a combination of the above lattices. This creates a simple-cubic lattice that alternates in the xy-plane (the plane of well pairing) between deep and shallow wells. The alternating in depths is a consequence of the ability to well pair smoothly.

When the correct phase parameters are changed, each deep well will pair with an adjacent shallow well, but depending on how the wells are split, they may or may not be allowed to exchange positions. The following illustrations show the combined 3D lattice and the "reverse" lattice where the deep/shallow wells have exchanged after the well pairing. The actual parameters that allow for this transformation will be explored in the next section.



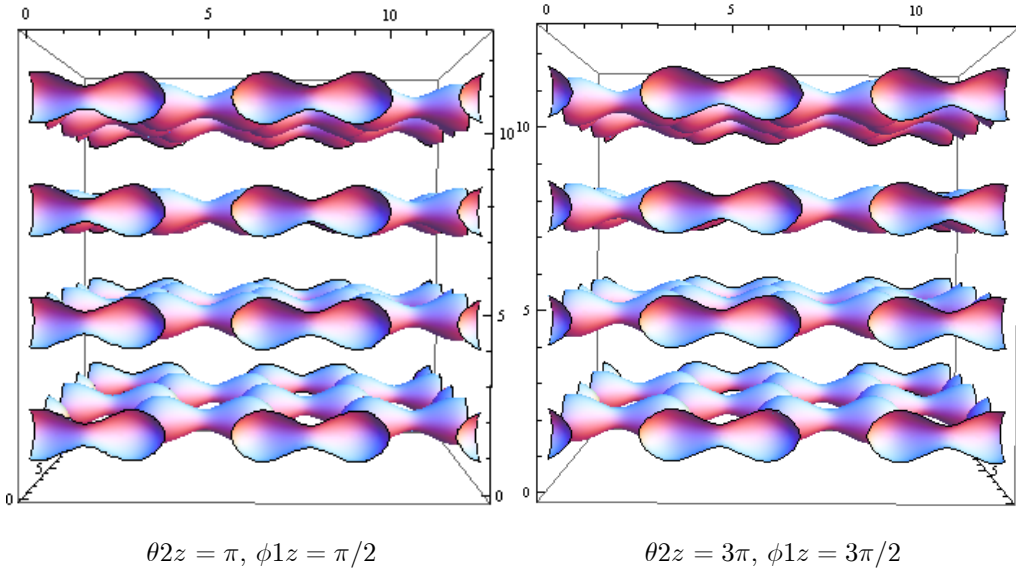
2.6 Linear Well Pairing

The simplest transformation of well pairing is pairing along a line, that is, limiting the pairing to one dimension. The lattice configuration shown above allows for easy well pairing

in one dimension, more difficult pairing in a second dimension, and no pairing in the third. The direction is arbitrary and determined by the values of the intensities. For example, the lattice shown above was created by the following values: $I_{1x} = I_{2y} = I_{3x}$, $I_{1x} = 5 * I_{1z}$, $I_{2y} = 5 * I_{2z}$, $I_{3x} = 3 * I_{3y}$ and $\theta_{3x} = \theta_{3y} = \pi$.

This particular lattice can easily pair wells in the \hat{x} -direction, can be made to pair in the \hat{y} -direction, and cannot pair in the \hat{z} . For pairing along a line, this lattice would be implemented to pair wells along the x-axis. This could also be used to split wells, starting first with wells paired to create deep wells and then separating them back into the separate wells. However, the separate wells will not be of the same size (depth), so this perhaps may not be the best option in practice.

Implementing the well pairing sequence is easy, we just let $\theta 2z$ go from 0 to π simultaneous with $\phi 1z$ going from 0 to $\pi/2$. The deep and shallow wells can then be made to exchange positions by allowing $\theta 2z$ and $\phi 1z$ to continue increasing or retain their positions by allowing $\theta 2z$ and $\phi 1z$ to decrease at the same rate as before.

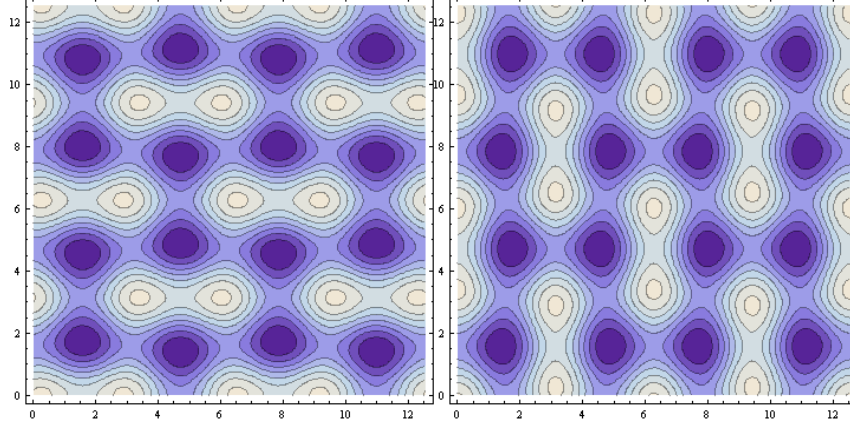


2.7 Circular Well Pairing

This transformation is of great interest, because it can be used to mimic the movement of charged particles within a magnetic field. Depending on which wells the particles begin in they can be made to move counter- or clockwise in a circle (really a square) of four wells by pairing, for instance, in the \hat{x} -direction, then the \hat{y} , then the $-\hat{x}$, then the $-\hat{y}$. This is a simple extension of the linear well pairing sequence.

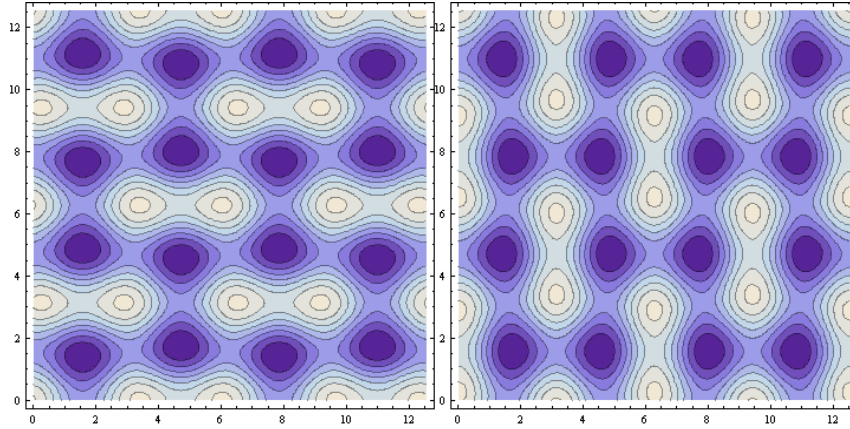
If we begin with the same lattice setup used in the previous section, we can first use the

linear pairing process of letting $\theta 2z$ go from zero to 2π and $\phi 1z$ go from 0 to π simultaneously. At this point the particle will have moved across one side of the square. Now we must adjust lattice parameters to "rotate" the pairing process by $\pi/2$.



$$\theta 2z = \pi, \phi 1z = \pi/2, \theta 1z = 0$$

$$\theta 2z = 4\pi, \phi 1z = \pi/2, \theta 1z = \pi$$



$$\theta 2z = 3\pi, \phi 1z = 3\pi/2, \theta 1z = 0$$

$$\theta 2z = 2\pi, \phi 1z = -\pi/2, \theta 1z = \pi$$

2.8 Extension and Future Research

The ultimate goal is to use dynamical lattices to transport loaded particles along controlled paths, such as the imitation of particles responding to magnetic fields via the circular well-pairing. Before this is possible, a stable method for varying the lattice potential to maintain predictable behavior in the particle wavefunctions must be determined. Creating an initial stationary wavefunction can be done by Taylor expanding (and retaining only the second-order term) about a well minimum to approximate a QHO potential

$$V_{QHO} \approx -\frac{V(0)x^2}{2}, \quad (33)$$

where the natural frequency of the trap is $\omega = \sqrt{V(0)/m}$. This allows us to prepare a particle in any stationary state for the QHO. The next step will be to find a manner of transforming the lattice such that the state is not perturbed by the evolving lattice potential. This exploration will likely have to be numeric, perhaps even a trial-and-error approach, as there are currently no known solutions to the Schrödinger equation for a potential of this lattice form.

With the ability to controllably transport loaded particles (in a way that can be easily repeated,) condensed matter and solid state phenomena such as superconductivity can be explored in a more directly observable way. Once these phenomena can be recreated artificially, the technological opportunities are vast.

Conclusions

This paper described how two-particle quantum states are resistant to excitations, maintaining about 80% to 90% probability of remaining in the ground state, even for fast interaction ramping and large interaction strengths. This is significant because experiments using such interactions can be confident in the probability of keeping loaded particles in the ground state during operations that involve changing the interaction strength.

Though the realm of quantum mechanics seems to bear no direct connection to the macroscopic world we occupy, the laws that govern the microscopic scales of the universe open a doorway to powerful new and untapped resources. Realization of advanced quantum technologies hinges upon our ability to fully understand the nature of the quantum world and how to control it. Our research attempts to glimpse into the reservoir of unexplored quantum behaviors so that its nature may be better understood.

3 Appendix A: Expanded Functions

3.1 Normalization Factor

$$N_n = \pi^{-1/2} \sqrt{\frac{\Gamma(\frac{3}{4} - \frac{\epsilon_n}{2})\Gamma(\frac{1}{4} - \frac{\epsilon_n}{2})}{\Phi(\frac{3}{4} - \frac{\epsilon_n}{2}) - \Phi(\frac{1}{4} - \frac{\epsilon_n}{2})}}$$

where Φ is the logarithmic derivative of the factorial function Γ .

3.2 Expanded Lattice Average Intensity

$$\begin{aligned} I_{avg} = & 2I_{1x}[1 + \cos(2ky - \theta_{1x})] + 2I_{1z}[1 + \cos(2ky - \theta_{1z})] + 2I_{2y}[1 + \cos(2kx - \theta_{2y})] \\ & + 2I_{2z}[1 + \cos(2kx - \theta_{2z})] + 2I_{3x}[1 + \cos(2kz - \theta_{3x})] + 2I_{3y}[1 + \cos(2kz - \theta_{3y})] \\ & + 2\sqrt{I_{1z}I_{2z}}[\cos(ky - kx + \phi_{1z}) + \cos(ky + kx + \phi_{1z} - \theta_{2z}) \\ & \quad + \cos(ky + kx - \theta_{1z} - \phi_{1z}) + \cos(ky - kx - \theta_{1z} - \phi_{1z} + \theta_{2z})] \\ & + 2\sqrt{I_{1x}I_{3x}}[\cos(ky - kz + \phi_{1x}) + \cos(ky + kz + \phi_{1x} - \theta_{3x}) \\ & \quad + \cos(ky + kz - \theta_{1x} - \phi_{1x}) + \cos(ky - kz - \theta_{1x} - \phi_{1x} + \theta_{3x})] \\ & + 2\sqrt{I_{2y}I_{3y}}[\cos(kx - kz + \phi_{2y}) + \cos(kx + kz + \phi_{2y} - \theta_{3y}) \\ & \quad + \cos(kx + kz - \theta_{2y} - \phi_{2y}) + \cos(kx - kz - \theta_{2y} - \phi_{2y} + \theta_{3y})] \end{aligned}$$

where $I_{2x} \propto E_{2x}^2$, etc., and k is the beam wavenumber.

References

- [1] T. Busch, B. Englert, K. Rzazewski, and M. Wilkens, "Two Cold Atoms in a Harmonic Trap," *Found. Phys.*, vol. 28, no. 4, 1998.
- [2] J. Viana-Gomes and N. M. R. Peres, "Solution of the quantum harmonic oscillator plus a delta-function potential at the origin: The *oddness* of its even-parity solutions," *Eur. J. Phys.*, vol. 32, no. 1377, 2011.
- [3] C. Chen, R. Grimm, P. Julienne, and E. Tiesinga, "Feshbach resonances in ultracold gases," *Rev. Mod. Phys.*, vol. 82, pp. 1226-1227, 2010.
- [4] M. Bubhardt and M. Freyberger, "Decoherent dynamics of two nonclassically correlated particles," *Phys. Rev. A*, vol. 75, no. 052101, 2007.
- [5] H. Mack and M. Freyberger, "Dynamics of entanglement between two trapped atoms," *Phys. Rev. A*, vol. 66, no. 042113, 2002.
- [6] K. Kormann, S. Holmgren, and H. O. Karlsson. "Accurate time propagation for the Schrödinger equation with an explicitly time-dependent Hamiltonian," *J. of Chem. Phys.*, vol. 128, no. 184101, 2008.
- [7] D. Menasche, "The Role of Mutually Attractive Interactions Between Neutral Atoms: A Split-Operator Method Analysis," *Senior Capstone*, American Univ., 2011.
- [8] P. Johnson, "Notes on quantum mechanical lattice representation," American Univ., 2011.
- [9] J. Sebby-Strabley, M. Anderlini, P. S. Jessen, and J. V. Porto, "Lattice of double wells for manipulating pairs of cold atoms," *Phys. Rev. A*, vol. 73, no. 033605, 2003.
- [10] M. Anderlini, J. Sebby-Strabley, J. Kruse, J. V. Porto, W. D. Phillips, "Controlled atom dynamics in a double-well optical lattice," *J. Phys. B.: At. Mol. Opt. Phys.*, vol. 39, 2006.
- [11] D. Jaksch, C. Bruder, J. I. Cirac, C. W. Gardiner, and P. Zoller, "Cold Bosonic Atoms in Optical Lattices," *Phys. Rev. Lett.*, vol. 81, no. 15, 1998.
- [12] M. Nielsen and I. Chuang, *Quantum Computation and Quantum Information*, 10th Anniv. Ed., pp. 60-78, 2010.
- [13] D. J. Griffiths, *Introduction to Quantum Mechanics*, 1995.